

Cylindrical Bending of Laminated Plates with Distributed and Segmented Piezoelectric Actuators/Sensors

Senthil S. Vel* and R. C. Batra†

Virginia Polytechnic Institute and State University, Blacksburg, Virginia 24061

The generalized plane quasistatic deformations of linear piezoelectric laminated plates are analyzed by the Eshelby–Stroh formalism. The laminate consists of homogeneous elastic or piezoelectric laminae of arbitrary thickness and width. The three-dimensional differential equations of equilibrium for a piezoelectric body are exactly satisfied at every point in the body. The analytical solution is in terms of an infinite series; the continuity conditions at the interfaces between adjoining laminae and boundary conditions at the edges are satisfied in the sense of Fourier series. The formulation admits different boundary conditions at the edges and is applicable to thick and thin laminated plates. Results are presented for laminated elastic plates with a distributed piezoelectric actuator on the upper surface and a sensor on the lower surface and subjected to different sets of boundary conditions at the edges. Results are also provided for a piezoelectric bimorph and an elastic plate with segmented piezoelectric actuators bonded to its upper and lower surfaces.

I. Introduction

IN recent years piezoelectric materials have been integrated with structural systems to form a class of smart structures. The piezoelectric materials are capable of altering the structure's response through sensing, actuation, and control. By integrating surface-bonded and embedded actuators into structural systems, desired localized strains may be induced by applying the appropriate voltage to the actuators.

Initial investigations of piezoelectric materials as actuators involved the control of vibrations of beams.^{1–3} To successfully incorporate piezoelectric actuators into structures, the mechanical interaction between the actuators and the base structure must be fully understood. Mechanical models have been developed by Crawley and de Luis,³ Crawley and Anderson,⁴ Im and Atluri,² and others for studying the interaction of piezoelectric patches surface-mounted to beams. Lee,⁵ Wang and Rogers,⁶ and Mitchell and Reddy⁷ have developed plate theories for composite laminates with piezoelectric actuators. Tzou and Zhong⁸ have developed a first-order shear deformation theory for piezoelectric shells. Numerous finite element studies have also been conducted (e.g., see Refs. 9–13).

Pagano^{14,15} obtained analytical solutions for simply supported linear elastic laminated plates. His method has been extended by numerous researchers to study the deformations of simply supported linear elastic laminated plates with embedded or surface-mounted distributed piezoelectric actuators (e.g., see Ray et al.,^{16–18} Heyliger and Brooks,¹⁹ Brooks and Heyliger,²⁰ Zhou and Tiersten,²¹ and Yang et al.²²). These solution techniques are valid only when the edges are simply supported, electrically grounded, and all layers are of equal width. Thus they are incapable of analyzing laminates with segmented actuators and/or when edges of the plate are either clamped or traction free. Brooks and Heyliger²⁰ and Batra et al.²³ simulate a segmented piezoelectric actuator by applying an electric potential only over a part of a distributed piezoelectric actuator.

Vel and Batra²⁴ have used the Eshelby–Stroh formalism to analyze the generalized plane strain deformations of laminated elastic plates subjected to arbitrary boundary conditions. Here we extend it to obtain analytical solutions for displacements, stresses, and electric fields for laminated plates with piezoelectric actuators and

sensors. The piezoelectric layers are treated as an integral part of the structure. A novel feature of the present method is its ability to analyze laminated plates with segmented actuators and sensors. As illustrated by the results for clamped-clamped and cantilever laminates, our formulation admits different boundary conditions. Three-dimensional equilibrium equations of linear piezoelectricity simplified to the case of generalized plane-strain deformations are solved by the Eshelby–Stroh formalism. Thus the governing equations are exactly satisfied, and various constants in the general solution are determined from the boundary and the continuity conditions at the interfaces. This results in an infinite system of equations in infinitely many unknowns. The truncation of this set of equations inevitably introduces some errors that can be minimized by increasing the number of terms in the series. The procedure is illustrated by computing results for the cylindrical bending of laminated elastic plates with a distributed piezoelectric actuator on the upper surface and a sensor on the lower surface and subjected to different sets of boundary conditions. Results are also provided for a piezoelectric bimorph and an elastic plate with segmented piezoelectric actuators bonded to its upper and lower surfaces. These results could be used to assess the accuracy of different plate theories and/or validating finite element codes.

II. Formulation of the Problem

We use a rectangular Cartesian coordinate system, shown in Fig. 1, to describe the infinitesimal quasistatic deformations of a piezoelectric laminate occupying the region $[L^{(1)}, L^{(N_3+1)}] \times (-\infty, \infty) \times [H^{(1)}, H^{(N_3+1)}]$ in the unstressed reference configuration. Planes $x_3 = H^{(1)}, \dots, H^{(n_3)}, \dots, H^{(N_3+1)}$ describe the bottom bounding surface, the horizontal interfaces between adjoining laminae, and the top bounding surface. Planes $x_1 = L^{(1)}, \dots, L^{(n_1)}, \dots, L^{(N_1+1)}$ are respectively the left bounding surface, the vertical interfaces between adjoining laminae, and the right bounding surface. If the region $[L^{(n_1)}, L^{(n_1+1)}] \times (-\infty, \infty) \times [H^{(n_3)}, H^{(n_3+1)}]$ is occupied by material, we refer to it as the (n_1, n_3) th lamina.

The equilibrium equations in the absence of body forces and free charges are

$$\sigma_{i,j} = 0, \quad D_{i,i} = 0 \quad (i, j = 1, 2, 3) \quad (1)$$

where σ_{ij} is the Cauchy stress tensor and D_i the electric displacement. A comma followed by index j indicates partial differentiation with respect to the present position x_j of a material particle, and a repeated index implies summation over the range of the index.

The constitutive equations of a linear piezoelectric medium are²⁵

$$\sigma_{ij} = C_{ijkl} u_{k,l} - e_{kij} E_k, \quad D_i = e_{ikl} u_{k,l} + \epsilon_{ik} E_k \quad (2)$$

Received 19 February 1999; revision received 30 August 1999; accepted for publication 9 September 1999. Copyright © 1999 by Senthil S. Vel and R. C. Batra. Published by the American Institute of Aeronautics and Astronautics, Inc., with permission.

*Postdoctoral Research Associate, Department of Engineering Science and Mechanics, MC 0219.

†Clifton C. Garvin Professor, Department of Engineering Science and Mechanics, MC 0219.

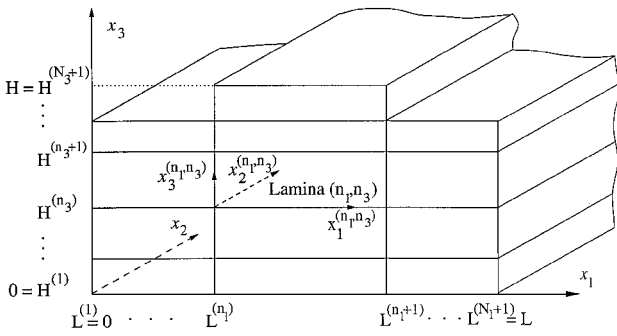


Fig. 1 Piezoelectric laminated plate.

where u_k is the mechanical displacement, E_k the electric field, C_{ijkl} the elasticity tensor, e_{kij} the piezoelectric moduli, and ϵ_{ik} the electric permittivity. The electric field is related to the electric potential ϕ by $E_i = -\phi_{,i}$. We will interchangeably use the direct and indirect notation. The material constants are assumed to exhibit the following symmetries $C_{ijkl} = C_{jikl} = C_{klij}$ and $e_{kij} = e_{kji}$. Material elasticities are assumed to yield a positive strain energy density for every nonrigid deformation of the body, that is,

$$C_{ijkl}u_{i,j}u_{k,l} > 0 \quad \text{if} \quad u_{i,j} + u_{j,i} \neq 0 \quad (3)$$

Moreover ϵ_{ik} is positive definite in the sense that $\epsilon_{ij}E_iE_j > 0$ for arbitrary real nonzero E_i .

The boundary or material interface conditions on the surface $x_3 = H^{(n_3)}$ of the (n_1, n_3) th lamina may be specified as follows:

1) If the surface is an interface between two laminae, then displacements, surface tractions, electric potential, and the normal component of the electric displacement between them are taken to be continuous, that is,

$$\begin{aligned} \llbracket \mathbf{u} \rrbracket &= \mathbf{0}, & \llbracket \boldsymbol{\sigma}_3 \rrbracket &= \mathbf{0}, & \llbracket \phi \rrbracket &= 0 \\ \llbracket D_3 \rrbracket &= 0 \quad \text{on} \quad x_3 = H^{(n_3)} \end{aligned} \quad (4)$$

Here $\llbracket \mathcal{F} \rrbracket$ denotes the jump in the value of \mathcal{F} across an interface and

$$(\boldsymbol{\sigma}_k)_i = \sigma_{ik} \quad (5)$$

Thus the adjoining laminae are presumed to be perfectly bonded together.

2) If the surface is an electroded interface, then the potential on this surface is a known function $f(x_1)$ while the normal component of the electric displacement need not be continuous across this interface, i.e.,

$$\llbracket \mathbf{u} \rrbracket = \mathbf{0}, \quad \llbracket \boldsymbol{\sigma}_3 \rrbracket = \mathbf{0}, \quad \phi = f(x_1) \quad \text{on} \quad x_3 = H^{(n_3)} \quad (6)$$

We assume that the electrode is of negligible thickness and ignore its mechanical influence on the structure.

3) If the surface is not in contact with any other lamina, then boundary conditions are specified as

$$\mathbf{J} \begin{pmatrix} \mathbf{u} \\ \phi \end{pmatrix} + \hat{\mathbf{J}} \begin{pmatrix} \boldsymbol{\sigma}_3 \\ D_3 \end{pmatrix} = f(x_1) \quad \text{on} \quad x_3 = H^{(n_3)} \quad (7)$$

The function $f(x_1)$ is prescribed, and $\mathbf{J}, \hat{\mathbf{J}}$ are 4×4 diagonal matrices with their elements functions of at most x_1 . For most applications these diagonal matrices have entries either zero or one such that $\mathbf{J} + \hat{\mathbf{J}} = \mathbf{I}$, where \mathbf{I} is the 4×4 identity matrix. For example, if the surface is electroded and the traction is prescribed, then $\mathbf{J} = \text{diag}[0, 0, 0, 1]$, and $\hat{\mathbf{J}} = \text{diag}[1, 1, 1, 0]$.

The boundary/interface conditions may be similarly specified on the other three bounding surfaces $x_3 = H^{(n_3+1)}$, $x_1 = L^{(n_1)}$, and $x_1 = L^{(n_1+1)}$. Note that our problem formulation allows for the length of a lamina to be less than the span L of the plate. Said differently, the region $H^{(n_3)} \leq x_3 \leq H^{(n_3+1)}$, $0 \leq x_1 \leq L$ could be divided into several sections by vertical planes with each section made of a different material.

We postulate that the displacement \mathbf{u} and the electrical potential ϕ are functions of x_1 and x_3 only, and thus the deformations of the laminate correspond to generalized plane state of deformation. This assumption is reasonable because the applied loads (mechanical and electrical) and material properties are independent of x_2 , and the body is of infinite extent in the x_2 direction.

III. Solution of the Problem

We use the Eshelby–Stroh^{26,27} formalism as described by Ting²⁸ to obtain a general solution of Eqs. (1) and (2). Boundary conditions (7) or interface conditions (4) or (6) will be used to find unknown constants in the general solution. We construct a local coordinate system $x_1^{(n_1, n_3)}, x_2^{(n_1, n_3)}, x_3^{(n_1, n_3)}$ with origin at the point $[L^{(n_1)}, 0, H^{(n_3)}]$ in the global coordinate system and the local axes parallel to the global axes. The length and thickness of the (n_1, n_3) th lamina are denoted by $l^{(n_1, n_3)} = L^{(n_1+1)} - L^{(n_1)}$, $h^{(n_1, n_3)} = H^{(n_3+1)} - H^{(n_3)}$. In this section we drop the superscripts (n_1, n_3) for convenience, understanding that all material constants and unknowns belong to this lamina.

A. General Solution

Assume that

$$\begin{pmatrix} \mathbf{u} \\ \phi \end{pmatrix} = \mathbf{a}f(z) \quad (8)$$

where $z = x_1 + px_3$, f is an arbitrary analytic function, and \mathbf{a}, p are possible complex constants to be determined. Substitution of Eq. (8) into Eq. (2) and the result into Eq. (1) gives

$$\mathbf{D}(p)\mathbf{a} = \mathbf{0} \quad (9)$$

where

$$\begin{aligned} \mathbf{D}(p) &= \mathbf{Q} + p(\mathbf{R} + \mathbf{R}^T) + p^2\mathbf{T} \\ \mathbf{Q} &= \begin{bmatrix} \mathbf{Q}^E & \mathbf{e}_{11} \\ \mathbf{e}_{11}^T & -\epsilon_{11} \end{bmatrix}, \quad \mathbf{R} = \begin{bmatrix} \mathbf{R}^E & \mathbf{e}_{31} \\ \mathbf{e}_{13}^T & -\epsilon_{13} \end{bmatrix}, \quad \mathbf{T} = \begin{bmatrix} \mathbf{T}^E & \mathbf{e}_{33} \\ \mathbf{e}_{33}^T & -\epsilon_{33} \end{bmatrix} \\ \mathbf{Q}_{ik}^E &= C_{i1k1}, \quad \mathbf{R}_{ik}^E = C_{i1k3}, \quad \mathbf{T}_{ik}^E = C_{i3k3}, \quad (\mathbf{e}_{ij})_k = e_{ijk} \end{aligned} \quad (10)$$

Problem (9) can be stated as the following algebraic eigenvalue problem:

$$\mathbf{N} \begin{pmatrix} \mathbf{a} \\ \mathbf{b} \end{pmatrix} = p \begin{pmatrix} \mathbf{a} \\ \mathbf{b} \end{pmatrix} \quad (11)$$

where

$$\begin{aligned} \mathbf{N} &= \begin{pmatrix} -\mathbf{T}^{-1}\mathbf{R}^T & \mathbf{T}^{-1} \\ \mathbf{R}\mathbf{T}^{-1}\mathbf{R}^T - \mathbf{Q} & -\mathbf{R}\mathbf{T}^{-1} \end{pmatrix} \\ \mathbf{b} &= (\mathbf{R}^T + p\mathbf{T})\mathbf{a} = -(1/p)(\mathbf{Q} + p\mathbf{R})\mathbf{a} \end{aligned} \quad (12)$$

Because C_{ijkl} and ϵ_{ik} are positive definite, p cannot be real.²⁸ There are eight eigenvalues consisting of four pairs of complex conjugates. Let $(p_\alpha, \mathbf{a}_\alpha)$, $(\alpha = 1, 2, \dots, 8)$ be eigensolutions of Eq. (11) such that

$$\text{Im}(p_\alpha) > 0, \quad p_{\alpha+4} = \bar{p}_\alpha, \quad \mathbf{a}_{\alpha+4} = \bar{\mathbf{a}}_\alpha \quad (\alpha = 1, 2, 3, 4) \quad (13)$$

where \bar{p}_α is the complex conjugate of p_α .

Assuming that the eigenvalues p_α are distinct, a general solution of Eqs. (1) and (2) obtained by superposing eight solutions of the form (8) is

$$\begin{pmatrix} \mathbf{u} \\ \phi \end{pmatrix} = \sum_{\alpha=1}^4 [\mathbf{a}_\alpha f_\alpha(z_\alpha) + \bar{\mathbf{a}}_\alpha f_{\alpha+4}(\bar{z}_\alpha)] \quad (14)$$

where f_α ($\alpha = 1, 2, \dots, 8$) are arbitrary analytic functions of their arguments and $z_\alpha = x_1 + p_\alpha x_3$.

Substitution of Eq. (14) into Eq. (2) yields

$$\begin{aligned} \begin{pmatrix} \sigma_1 \\ D_1 \end{pmatrix} &= \sum_{\alpha=1}^4 [-p_\alpha \mathbf{b}_\alpha f'_\alpha(z_\alpha) - \bar{p}_\alpha \bar{\mathbf{b}}_\alpha f'_{\alpha+4}(\bar{z}_\alpha)] \\ \begin{pmatrix} \sigma_3 \\ D_3 \end{pmatrix} &= \sum_{\alpha=1}^4 [\mathbf{b}_\alpha f'_\alpha(z_\alpha) + \bar{\mathbf{b}}_\alpha f'_{\alpha+4}(\bar{z}_\alpha)] \end{aligned} \quad (15)$$

B. General Solution for Degenerate Piezoelectric Materials

The general solution just given is applicable for materials that possess distinct eigenvalues p_α ($\alpha = 1, 2, 3, 4$). When one of the eigenvalues, say p_1 , is repeated twice, there may or may not be two corresponding independent eigenvectors. If there exist two independent eigenvectors \mathbf{a}_1 and \mathbf{a}_2 associated with p_1 , then the general solution may be written as Eqs. (14) and (15) with p_2 set equal to p_1 .

If there exists only one independent eigenvector \mathbf{a}_1 associated with the double root p_1 , then a second independent solution is

$$\begin{pmatrix} \mathbf{u} \\ \phi \end{pmatrix} = \frac{d}{dp_1} [a_1 f_2(z_1)] = \frac{d\mathbf{a}_1}{dp_1} f_2(z_1) + \mathbf{a}_1 \frac{df_2(z_1)}{dp_1} \quad (16)$$

where $d\mathbf{a}_1/dp_1$ is obtained by differentiating Eq. (9):

$$\mathbf{D} \frac{d\mathbf{a}_1}{dp_1} + \frac{d\mathbf{D}}{dp_1} \mathbf{a}_1 = \mathbf{0} \quad (17)$$

The existence of a solution of Eq. (9) and (17) for \mathbf{a}_1 and $d\mathbf{a}_1/dp_1$ has been discussed by Yang et al.²⁹ and Dempsey and Sinclair.³⁰ Yang et al.²⁹ have shown that a nontrivial solution exists for \mathbf{a}_1 and $d\mathbf{a}_1/dp_1$. Therefore, the general solution is

$$\begin{pmatrix} \mathbf{u} \\ \phi \end{pmatrix} = \sum_{\alpha=1}^4 [a_\alpha f_\alpha(z_\alpha) + \bar{a}_\alpha f_{\alpha+4}(\bar{z}_\alpha)] + \mathbf{a}_1 \frac{df_2(z_1)}{dp_1} + \bar{\mathbf{a}}_1 \frac{df_6(\bar{z}_1)}{d\bar{p}_1} \quad (18)$$

where p_2 , z_2 , and \mathbf{a}_2 are defined to be equal to p_1 , z_1 , and $d\mathbf{a}_1/dp_1$, respectively. The corresponding general solution for the stress tensor and electric displacement is obtained by substituting Eq. (18) into Eq. (2). Degenerate materials with eigenvalues repeated three or four times can be similarly analyzed.

C. Series Solution

Even though Eq. (14) satisfies the equilibrium equations (1) for all choices of the analytic functions f_α , a choice based on the geometry of the problem and boundary conditions will simplify the work involved in solving a particular boundary-value problem. We select for the (n_1, n_3) th lamina

$$\begin{aligned} f_\alpha(z_\alpha) &= \sum_{m=0}^{\infty} \{v_{m\alpha}^{(1)} \exp(\eta_{m\alpha} z_\alpha) + w_{m\alpha}^{(1)} \exp[\eta_{m\alpha}(l - z_\alpha)]\} \\ &+ \sum_{k=0}^{\infty} \{v_{k\alpha}^{(3)} \exp(\lambda_{k\alpha} z_\alpha) + w_{k\alpha}^{(3)} \exp[\lambda_{k\alpha}(p_\alpha h - z_\alpha)]\} \\ f_{\alpha+4}(\bar{z}_\alpha) &= \overline{f_\alpha(z_\alpha)} \quad (\alpha = 1, 2, 3, 4) \end{aligned} \quad (19)$$

where $z_\alpha = x_1 + p_\alpha x_3$, $0 \leq x_1 \leq l$, $0 \leq x_3 \leq h$,

$$\eta_{m\alpha} = \begin{cases} -\frac{m_0 \pi i}{p_\alpha h} & \text{if } m = 0 \\ -\frac{m \pi i}{p_\alpha h} & \text{if } m \geq 1 \end{cases}, \quad \lambda_{k\alpha} = \begin{cases} \frac{k_0 \pi i}{l} & \text{if } k = 0 \\ \frac{k \pi i}{l} & \text{if } k \geq 1 \end{cases} \quad (20)$$

$i = \sqrt{-1}$ and $m_0, k_0 \in (0, 1)$. The functions involving m_0 and k_0 play the role of the constant term in a Fourier series expansion.

The function $\exp(\eta_{m\alpha} z_\alpha)$ in Eq. (19) varies sinusoidally on the surface $x_1 = 0$ of the (n_1, n_3) th lamina and decays exponentially in the x_1 direction. With increasing k , higher harmonics are introduced on the surface $x_1 = 0$ accompanied by steeper exponential decay in the x_1 direction. Similarly, functions $\exp[\eta_{m\alpha}(l - z_\alpha)]$, $\exp(\lambda_{k\alpha} z_\alpha)$

and $\exp[\lambda_{k\alpha}(p_\alpha h - z_\alpha)]$ vary sinusoidally on surfaces $x_1 = l$, $x_3 = 0$, and $x_3 = h$, respectively. The inequality in Eq. (13)₁ ensures that all functions decay exponentially toward the interior of the lamina. The choice (19)₂ for $f_{\alpha+4}(\bar{z}_\alpha)$ ensures that the mechanical displacement, stress tensor, electric potential, and electric displacement are real valued.

The unknowns $v_{k\alpha}^{(s)}$, $w_{k\alpha}^{(s)}$, ($s = 1, 3$) are assumed to be complex for $k \neq 0$ and real when $k = 0$. The superscript s indicates that the exponential function associated with the unknown has a sinusoidal variation on the surface $x_s = \text{constant}$. For nondegenerate materials substitution for f_α from Eq. (19) into Eq. (14) results in the following expression for the mechanical displacement and electric potential:

$$\begin{aligned} \begin{pmatrix} \mathbf{u} \\ \phi \end{pmatrix} &= A \left(\sum_{m=0}^{\infty} \{ \langle \exp(\eta_{m*} z_*) \rangle v_m^{(1)} + \langle \exp[\eta_{m*}(l - z_*)] \rangle w_m^{(1)} \} \right. \\ &+ \sum_{k=0}^{\infty} \{ \langle \exp(\lambda_{k*} z_*) \rangle v_k^{(3)} + \langle \exp[\lambda_{k*}(p_* h - z_*)] \rangle w_k^{(3)} \} \\ &+ \text{conjugate} \end{aligned} \quad (21)$$

where

$$\begin{aligned} A &= [\mathbf{a}_1, \mathbf{a}_2, \mathbf{a}_3, \mathbf{a}_4], \quad \langle g(z_*) \rangle = \text{diag}[g(z_1), g(z_2), g(z_3), g(z_4)] \\ [\mathbf{v}_m^{(s)}]_\alpha &= v_{m\alpha}^{(s)}, \quad [\mathbf{w}_m^{(s)}]_\alpha = w_{m\alpha}^{(s)}, \quad \alpha = 1, \dots, 4 \end{aligned}$$

and conjugate stands for the complex conjugate of the explicitly stated terms. The following expressions for stress components and electric displacement for nondegenerate materials are obtained by substituting Eq. (19) into Eq. (15):

$$\begin{aligned} \begin{pmatrix} \sigma_1 \\ D_1 \end{pmatrix} &= B \left(\sum_{m=0}^{\infty} \{ -\langle p_* \eta_{m*} \exp(\eta_{m*} z_*) \rangle w_m^{(1)} \right. \\ &+ \langle p_* \eta_{m*} \exp[\eta_{m*}(l - z_*)] \rangle w_m^{(1)} \} \\ &+ \sum_{k=0}^{\infty} \{ -\langle p_* \lambda_{k*} \exp(\lambda_{k*} z_*) \rangle v_k^{(3)} \\ &+ \langle p_* \lambda_{k*} \exp[\lambda_{k*}(p_* h - z_*)] \rangle w_k^{(3)} \} \Big) + \text{conjugate} \end{aligned} \quad (22)$$

$$\begin{aligned} \begin{pmatrix} \sigma_3 \\ D_3 \end{pmatrix} &= B \left(\sum_{m=0}^{\infty} \{ \langle \eta_{m*} \exp(\eta_{m*} z_*) \rangle v_m^{(1)} \right. \\ &- \langle \eta_{m*} \exp[\eta_{m*}(l - z_*)] \rangle w_m^{(1)} \} \\ &+ \sum_{k=0}^{\infty} \{ \langle \lambda_{k*} \exp(\lambda_{k*} z_*) \rangle v_k^{(3)} - \langle \lambda_{k*} \exp[\lambda_{k*}(p_* h - z_*)] \rangle w_k^{(3)} \} \\ &+ \text{conjugate} \end{aligned} \quad (23)$$

where $B = [\mathbf{b}_1, \mathbf{b}_2, \mathbf{b}_3, \mathbf{b}_4]$.

For degenerate materials the expressions (19) for analytic functions f_α remain the same, but the expressions for the mechanical displacement and electric potential are obtained by substituting for f_α from Eq. (19) into Eq. (18) instead of Eq. (14).

IV. Satisfaction of Boundary and Interface Conditions

Each lamina has its own set of unknowns $v_k^{(s)}$, $w_k^{(s)}$ ($s = 1, 3$). These unknowns are determined by imposing the interface continuity conditions and boundary conditions on all surfaces of the laminate by the classical Fourier series method. For example, let boundary conditions (7) be specified on the surface $x_3^{(1,1)} = 0$ of lamina (1, 1). We multiply Eq. (7) by $\exp[j\pi i x_1^{(1,1)} / l^{(1,1)}]$ and integrate

with respect to $x_1^{(1,1)}$ from $-l^{(1,1)}$ to $l^{(1,1)}$ to obtain

$$\int_{-l^{(1,1)}}^{l^{(1,1)}} \left\{ \mathcal{J}^{(1,1)} \left(\begin{matrix} \mathbf{u} \\ \phi \end{matrix} \right)^{(1,1)} + \mathcal{J}^{(1,1)} \left(\begin{matrix} \sigma_3 \\ D_3 \end{matrix} \right)^{(1,1)} - \mathcal{J}^{(1,1)} [x_1^{(1,1)}] \right\} \times \exp \left[j \frac{\pi i x_1^{(1,1)}}{l^{(1,1)}} \right] dx_1^{(1,1)} = \mathbf{0} \quad (24)$$

on $x_3^{(1,1)} = 0$ for $j = 0, 1, 2, \dots$. In Eq. (24) the functions multiplying the coefficients $\mathbf{v}_k^{(3)}$, $\mathbf{w}_k^{(3)}$ ($k \neq 0$) of the (1, 1) lamina have a sinusoidal variation in the x_1 direction and are extended over the interval $[-l^{(1,1)}, 0]$ without modification because they form the basis functions on this surface. The functions multiplying $\mathbf{v}_k^{(1)}$, $\mathbf{w}_k^{(1)}$ have an exponential variation in the x_1 direction; these are extended as even functions over the interval $[-l^{(1,1)}, 0]$. The functions multiplying $\mathbf{v}_0^{(3)}$, $\mathbf{w}_0^{(3)}$ are also extended as even functions because they play the role of the constant term in the Fourier series expansion. The known function $\mathcal{J}^{(1,1)} [x_1^{(1,1)}]$ is extended in a suitable manner. If the surface $x_3^{(1,1)} = 0$ is an interface between two adjoining laminae, then the conditions (4) or (6) need to be enforced instead of Eq. (7). Thus, upon imposing the boundary/interface conditions on all four bounding surfaces of every lamina in the laminated plate, we obtain an infinite system of linear algebraic equations for the infinitely many unknown coefficients. A general theory for the solution of the resulting infinite set of algebraic equations does not exist. However, reasonably accurate results may be obtained by truncating the series with summation indices m and k in Eq. (19) to $M^{(n_1, n_3)}$ and $K^{(n_1, n_3)}$ terms respectively for the (n_1, n_3) lamina. In general, we try to maintain approximately the same period of the largest harmonic on all the bounding surfaces of the lamina by choosing $K^{(n_1, n_3)} = \text{Ceil}[Kl^{(n_1, n_3)}/L]$ and $M^{(n_1, n_3)} = \text{Ceil}[Kh^{(n_1, n_3)}/L]$, where $\text{Ceil}(y)$ equals the smallest integer greater than or equal to y . Thus the total number of unknowns will depend solely on the choice of K .

From the structure of solution (21–23), the component functions decrease exponentially from the boundary/interfaces into the interior of the (n_1, n_3) th lamina. By truncating the series, we have effectively ignored coefficients with suffices greater than a particular value and approximated the coefficients that have small suffices. Because of the rapid decay of component functions associated with large suffices, the truncation of the series will not greatly influence the solution at the interior points. A larger value of K will give a more accurate solution at points close to the boundaries and interfaces. The coefficients $\mathbf{v}_m^{(1)}$ and $\mathbf{w}_m^{(1)}$ in Eqs. (22) and (23) are multiplied by η_{m*} while $\mathbf{v}_k^{(3)}$ and $\mathbf{w}_k^{(3)}$ are multiplied by λ_{k*} . However, the coefficients of these terms in the expressions (21) for displacements are unity. Because η_{m*} and λ_{k*} increase as the suffices m and k increase, the terms with large suffices are more significant for the stresses than for the displacements. Thus the stresses will converge more slowly than the displacements.

Once the unknown coefficients have been evaluated by solving the truncated system of linear equations, the displacements and stresses in each lamina are obtained from Eqs. (21–23). The stress component σ_{22} and the electric displacement component D_2 missing in Eqs. (22) and (23) are determined from Eq. (2).

V. Results and Discussion

The program developed for numerical computations was validated by comparing our results with those of Dube et al.³¹ and Heyliger and Brooks¹⁹ for simply supported piezoelectric plates; the two sets of results matched very well.

For all laminated plates considered in this section, each lamina is either made of graphite-epoxy or PZT-5A with nonzero material properties, taken from Xu and Noor,³² listed in Table 1. In the present analysis we treat the graphite-epoxy layer as a piezoelectric material with the piezoelectric moduli set equal to zero. Thus we also solve for the electric field in the graphite-epoxy layer, which is uncoupled from the elastic field.

A. Elastic Plate with Distributed PZT Actuators and Sensors

We consider a three-ply graphite-epoxy substrate with PZT-5A layers attached to its top and bottom surfaces. All five laminae of the

Table 1 Nonvanishing material properties of the graphite-epoxy and PZT-5A layers

| Material property | Graphite-epoxy 0-deg layer | PZT-5A layer |
|---|-------------------------------|-----------------|
| C_{1111} , GPa | 183.443 | 99.201 |
| C_{2222} , GPa | 11.662 | 99.201 |
| C_{3333} , GPa | 11.662 | 86.856 |
| C_{1122} , GPa | 4.363 | 54.016 |
| C_{1133} , GPa | 4.363 | 50.778 |
| C_{2233} , GPa | 3.918 | 50.778 |
| C_{2323} , GPa | 2.870 | 21.100 |
| C_{3131} , GPa | 7.170 | 21.100 |
| C_{1212} , GPa | 7.170 | 22.593 |
| e_{311} , Cm ⁻² (d_{311} , 10 ⁻¹² m/V) | 0 | -7.209 (-171) |
| e_{322} , Cm ⁻² (d_{322} , 10 ⁻¹² m/V) | 0 | -7.209 (-171) |
| e_{333} , Cm ⁻² (d_{333} , 10 ⁻¹² m/V) | 0 | 15.118 (374) |
| e_{223} , Cm ⁻² (d_{223} , 10 ⁻¹² m/V) | 0 | 12.322 (292) |
| e_{113} , Cm ⁻² (d_{113} , 10 ⁻¹² m/V) | 0 | 12.322 (292) |
| ϵ_{11} , 10 ⁻⁸ F/m | 1.53 | 1.53 |
| ϵ_{22} , 10 ⁻⁸ F/m | 1.53 | 1.53 |
| ϵ_{33} , 10 ⁻⁸ F/m | 1.53 | 1.50 |

hybrid laminate are of equal width and extend from $x_1 = 0$ to L . The following two lamination schemes for the substrate are considered:

1) A cross-ply scheme where the fibers are oriented parallel to the x_1 , x_2 , and x_1 directions in the bottom, middle, and top layers, respectively, i.e., a [PZT/0/90/0/PZT] laminate.

2) An angle-ply scheme where the fibers are oriented at 45, -45, and 45 deg with respect to the x_1 axis on the x_1 - x_2 plane in the bottom, middle, and top layers, respectively, i.e., a [PZT/45/-45/45/PZT] laminate.

The graphite-epoxy laminae are of thickness $H/4$ while the PZT-5A laminae are of thickness $H/8$. The locations of the bottom surface, the four interfaces, and the top surface are

$$[H^{(1)}, H^{(2)}, H^{(3)}, H^{(4)}, H^{(5)}, H^{(6)}] = [0, 1, 3, 5, 7, 8]H/8 \quad (25)$$

The interfaces between the PZT laminae and their neighboring graphite-epoxy laminae are electroded and held at zero electric potential, i.e., interface conditions (6) are applied at $x_3 = H^{(2)}$ and $H^{(5)}$ with $f(x_1) = 0$. The graphite-epoxy laminae are assumed to be perfectly bonded to each other, and interface conditions (4) are enforced on the surfaces $x_3 = H^{(3)}$ and $H^{(4)}$. The bottom surface $x_3 = 0$ is traction free and is in contact with air, thus permitting us to prescribe $\mathcal{J}^{(1,1)} = \mathbf{0}$, $\mathcal{J}^{(1,1)} = \mathbf{I}$, and $f(x_1) = \mathbf{0}$. The top surface $x_3 = H$ is electroded, and the following electromechanical loads are considered.

1) Mechanical load:

$$\sigma_3(x_1, H) = q_0[0, 0, \sin(\pi x_1/L)]^T, \quad \phi(x_1, H) = 0 \quad (26)$$

2) Electrical load:

$$\phi(x_1, H) = \phi_0 \sin(\pi x_1/L), \quad \sigma_3(x_1, H) = \mathbf{0} \quad (27)$$

Results for combined mechanical and electrical loads on the surface $x_3 = H$ can be obtained by superposition of the solutions corresponding to the load 1 and 2. Results for any mechanical or electrical load can be computed by expanding the load into a Fourier series and superposing the results for each Fourier component. In the case of an electric load, the top PZT lamina may be considered to be an actuator. For both loading cases a potential may be induced on the surface $x_3 = 0$ of the PZT lamina bonded to the bottom surface of the substrate. This PZT layer may be considered as a sensor. The edges $x_1 = 0, L$ are held at zero electric potential and subjected to various mechanical boundary conditions. These edges may be either clamped (C) with $u_1 = u_2 = u_3 = 0$ or free of traction (F) with $\sigma_{11} = \sigma_{12} = \sigma_{13} = 0$ or simply supported (S) with $\sigma_{11} = \sigma_{12} = 0, u_3 = 0$. The boundary conditions used at a simply supported edge are identical to those used by Pagano.¹⁵ If the surface $x_1 = 0$ is clamped and the surface $x_1 = L$ is traction free, i.e., a cantilever laminate, we denote the configuration as CF . Similarly CC and SS denote laminates that are clamped or simply supported respectively on both edges.

Table 2 Convergence study for the angle-ply cantilever hybrid laminate subjected to mechanical load ($L/H = 5$)

| K | \bar{u}_1 ($L/4, H$) | \bar{u}_3 ($L/2, 5H^\pm/8$) | $\bar{\sigma}_{11}$ ($L/2, H$) | $\bar{\sigma}_{13}$ ($L/4, 7H^\pm/8$) | $\bar{\sigma}_{23}$ ($3L/4, 5H^\pm/8$) | $\bar{\sigma}_{33}$ ($L/2, 3H^\pm/8$) | $\bar{\sigma}_{33}$ ($L/2, H/2$) | $\bar{\phi}$ ($L/2, 0$) | \bar{D}_3 ($L/2, H$) |
|-----|-----------------------------|------------------------------------|-------------------------------------|--|---|--|---------------------------------------|------------------------------|-----------------------------|
| 100 | -6.2601 | 7.7277 | -2.4675 | 0.4028 | 0.7286 | 0.2989 | 0.5094 | 0.1708 | 0.2151 |
| 200 | -6.2848 | 7.7277 | -2.6404 | 0.4120 | 0.7199 | 0.3900 | 0.5094 | 0.1727 | 0.2082 |
| 300 | -6.2891 | 7.7482 | -2.6871 | 0.4260 | 0.7332 | 0.3244 | 0.5094 | 0.1732 | 0.2068 |
| 400 | -6.2908 | 7.7482 | -2.6871 | 0.4219 | 0.7364 | 0.3601 | 0.5094 | 0.1732 | 0.2068 |
| 500 | -6.2917 | 7.7515 | -2.7096 | 0.4152 | 0.7378 | 0.3315 | 0.5094 | 0.1734 | 0.2058 |
| | | 7.7515 | -2.7096 | 0.4178 | 0.7360 | 0.3528 | 0.5094 | 0.1736 | |
| | | 7.7527 | -2.7217 | 0.4220 | 0.7369 | 0.3477 | 0.5094 | | |
| | | 7.7527 | | 0.4203 | 0.7381 | 0.3495 | | | |
| | | 7.7533 | | 0.4171 | 0.7386 | 0.3366 | | | |
| | | 7.7533 | | 0.4185 | 0.7377 | 0.3477 | | | |

Table 3 Convergence study for the angle-ply cantilever hybrid laminate subjected to electrical load ($L/H = 5$)

| K | \hat{u}_1 ($L/4, H$) | \hat{u}_3 ($L/2, 5H^\pm/8$) | $\hat{\sigma}_{11}$ ($L/2, H$) | $\hat{\sigma}_{13}$ ($L/4, 7H^\pm/8$) | $\hat{\sigma}_{23}$ ($3L/4, 5H^\pm/8$) | $\hat{\sigma}_{33}$ ($L/2, 3H^\pm/8$) | $\hat{\sigma}_{33}$ ($L/2, H/2$) | $\hat{\phi}$ ($L/2, 0$) | \hat{D}_3 ($L/2, H$) |
|-----|-----------------------------|------------------------------------|-------------------------------------|--|---|--|---------------------------------------|------------------------------|-----------------------------|
| 100 | 1.7678 | -1.7968 | -1.4694 | -3.9404 | -2.5429 | 2.8036 | 3.3889 | -0.0277 | -1.0867 |
| 200 | 1.7851 | -1.7968 | -1.4564 | -3.9283 | -2.5354 | 2.3079 | 3.3889 | -0.0278 | -1.0864 |
| 300 | 1.7888 | -1.8129 | -1.4528 | -3.9731 | -2.5486 | 2.6584 | 3.3888 | -0.0279 | -1.0863 |
| 400 | 1.7901 | -1.8129 | -1.4511 | -3.9764 | -2.5520 | 2.4610 | 3.3888 | -0.0279 | -1.0862 |
| 500 | 1.7909 | -1.8161 | -1.4502 | -3.9575 | -2.5505 | 2.6180 | 3.3888 | -0.0279 | -1.0862 |
| | | -1.8161 | | -3.9575 | -2.5485 | 2.4971 | 3.3888 | | |
| | | -1.8173 | | -3.9685 | -2.5509 | 2.5986 | 3.3888 | | |
| | | -1.8173 | | -3.9682 | -2.5523 | 2.5146 | 3.3888 | | |
| | | -1.8180 | | -3.9599 | -2.5513 | 2.5878 | 3.3888 | | |
| | | -1.8180 | | -3.9598 | -2.5502 | 2.5235 | 3.3888 | | |

The effect of the truncation of the series is investigated for a cantilever laminate subjected to electromechanical loads. Computed results for various quantities at specific points in the laminate are listed in Table 2 for the mechanical load. The following nondimensionalization has been used:

$$\begin{aligned}
 (\bar{u}_1, \bar{u}_3) &= 100 \left(\frac{L}{H} u_1, u_3 \right) \frac{E_T H^3}{L^4 q_0}, & \bar{\sigma}_{11} &= 10 \frac{\sigma_{11} H^2}{L^2 q_0} \\
 (\bar{\sigma}_{13}, \bar{\sigma}_{23}, \bar{\sigma}_{33}) &= \left(\frac{\sigma_{13} H}{q_0 L}, 10 \frac{\sigma_{23} H}{q_0 L}, \frac{\sigma_{33}}{q_0} \right) \\
 \bar{\phi} &= 100 \frac{\phi d_T E_T H}{L^2 q_0}, & \bar{D}_3 &= \frac{D_3 H^2}{d_T L^2 q_0}
 \end{aligned} \quad (28)$$

where $E_T = 10.3$ GPa and $d_T = 374 \times 10^{-12}$ m/V. The displacements \bar{u}_1, \bar{u}_3 , transverse shear stresses $\bar{\sigma}_{13}, \bar{\sigma}_{23}$ across the interfaces, the electric potential $\bar{\phi}$, and the electric displacement \bar{D}_3 converge quickly, but the axial stress $\bar{\sigma}_{11}$ and the transverse normal stress $\bar{\sigma}_{33}$ across the interface $x_3 = 3H/8$ converge slowly. However, the transverse normal stress at the midpoint of the laminate shows rapid convergence.

Table 3 presents a convergence study for a cantilever laminate subjected to electrical load where the nondimensional variables are defined as

$$\begin{aligned}
 (\hat{u}_1, \hat{u}_3) &= 10 \left(\frac{u_1 H}{L}, u_3 \right) \frac{H^2}{L^2 d_T \phi_0}, & \hat{\sigma}_{11} &= \frac{\sigma_{11} H}{10 E_T d_T \phi_0} \\
 (\hat{\sigma}_{13}, \hat{\sigma}_{23}, \hat{\sigma}_{33}) &= \left(\sigma_{13}, 10 \sigma_{23}, \frac{L}{H} \sigma_{33} \right) \frac{L}{E_T d_T \phi_0} \\
 \hat{\phi} &= \frac{\phi}{\phi_0}, & \hat{D}_3 &= \frac{D_3 H}{100 E_T d_T^2 \phi_0}
 \end{aligned} \quad (29)$$

Table 3 shows that $\hat{\sigma}_{33}$ on the interface $x_3 = 3H/8$ converges slowly, whereas the other components of the stress tensor, the mechanical displacements, the electric potential, and the electric displacement converge rapidly.

The distribution of the transverse shear stress $\bar{\sigma}_{13}$ at four sections $x_1/L = 0.1, 0.25, 0.75,$ and 0.9 along the span of a cross-ply cantilever laminate is shown in Fig. 2a for the case of mechanical load.

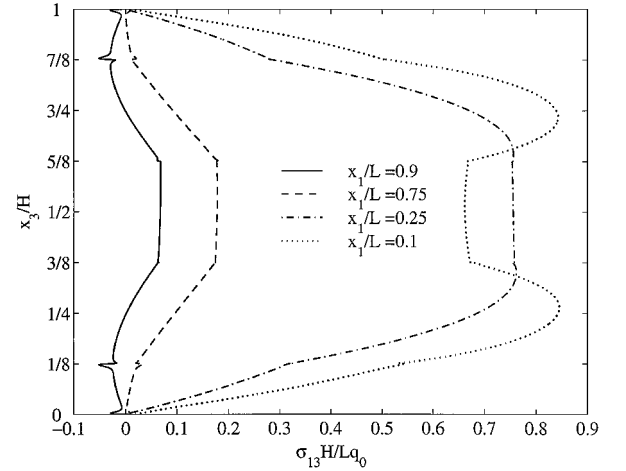
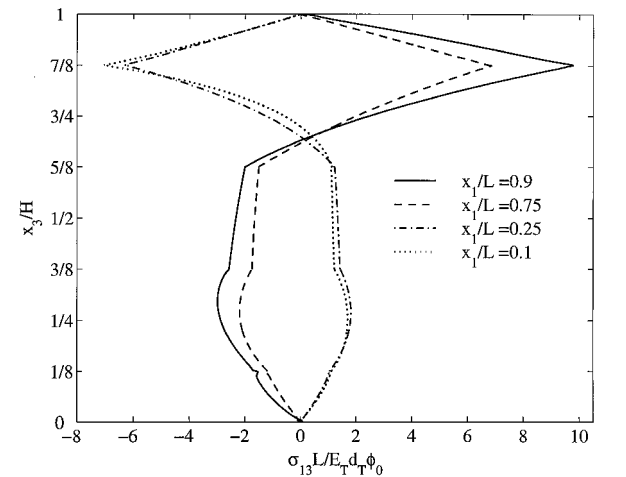
**a) Mechanical load****b) Electrical load****Fig. 2** Transverse shear-stress distribution on four sections for a cantilever cross-ply hybrid laminate ($L/H = 5$).

Table 4 Mechanical displacement, stresses, electrical potential, and electric displacement for six configurations ($L/H = 5$, $K = 500$ terms)

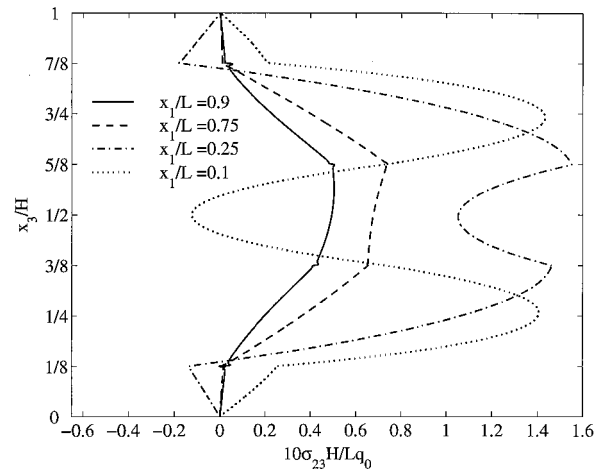
| Variable | SS cross ply | SS angle ply | CC cross ply | CC angle ply | CF cross ply | CF angle ply |
|----------------------------------|-----------------|-----------------|-----------------|-----------------|-----------------|-----------------|
| $\bar{u}_1(L/4, H)$ | -1.580 | -2.369 | -0.708 | -0.864 | -4.119 | -6.292 |
| $\bar{u}_3(L/2, H/2)$ | 2.276 | 3.010 | 1.249 | 1.436 | 5.667 | 7.741 |
| $\bar{\sigma}_{11}(L/2, H)$ | 5.171 | 7.600 | 2.811 | 3.470 | -0.701 | -2.722 |
| $\bar{\sigma}_{13}(L/8, H/2)$ | 0.427 | 0.408 | 0.321 | 0.377 | 0.707 | 0.804 |
| $\bar{\sigma}_{23}(7L/8, 3H/4)$ | 0.000 | -0.693 | 0.000 | -0.593 | 0.000 | 0.246 |
| $\bar{\sigma}_{33}(L/2, H/2)$ | 0.506 | 0.510 | 0.507 | 0.509 | 0.507 | 0.509 |
| $\bar{\phi}(L/2, 0)$ | -0.233 | -0.352 | -0.106 | -0.136 | 0.074 | 0.174 |
| $\bar{D}_3(L/2, H)$ | -0.215 | -0.343 | -0.091 | -0.125 | 0.096 | 0.206 |
| $\hat{u}_1(L/4, H)$ | -3.549 | -6.238 | -1.342 | -2.148 | 0.821 | 1.791 |
| $\hat{u}_3(L/2, H/2)$ | 2.398 | 3.746 | 0.705 | 0.887 | -0.824 | -1.809 |
| $\hat{\sigma}_{11}(L/2, H)$ | -2.253 | -1.436 | -2.855 | -2.547 | -2.257 | -1.450 |
| $\hat{\sigma}_{13}(L/4, 15H/16)$ | -3.218 | -2.128 | -3.056 | -1.854 | -3.046 | -1.836 |
| $\hat{\sigma}_{23}(7L/8, 3H/4)$ | 0.000 | -1.746 | 0.000 | -0.840 | 0.000 | -1.604 |
| $\hat{\sigma}_{33}(L/2, H/2)$ | 3.167 | 3.477 | 3.109 | 3.215 | 3.176 | 3.389 |
| $\hat{\phi}(L/2, 0)$ | -0.019 | -0.028 | -0.007 | -0.008 | -0.019 | -0.028 |
| $\hat{D}_3(L/2, H)$ | -1.040 | -1.087 | -1.007 | -1.025 | -1.040 | -1.086 |

The shear-stress distribution at a section close to the clamped edge attains a maximum near the middle of the 0-deg lamina. However, at sections close to the free edge $\bar{\sigma}_{13}$ is maximum at a point on the interface between two laminae. The corresponding transverse shear-stress distributions for the electrical loading are shown in Fig. 2b. In this case the transverse shear stress is largest on the interface $x_3 = 7H/8$ between the PZT actuator and the neighboring graphite-epoxy lamina. Furthermore, the transverse shear stress exhibits an affine behavior through the thickness of the PZT actuator. The results plotted in Figs. 2a and 2b clearly show that the computed transverse shear-stress distributions satisfy the interface continuity conditions very well and also vanish on the top and bottom long faces of the hybrid laminate. The nondimensional $\bar{\sigma}_{23}$ distributions on four sections along the span of an angle-ply laminate are shown in Figs. 3a and 3b for the mechanical and electrical loads, respectively. The through-thickness distribution of $\bar{\sigma}_{23}$ exhibits a very different profile as compared to that of $\bar{\sigma}_{13}$ in Fig. 2. When subjected to the electric load, $\bar{\sigma}_{23}$ is largest at the interface $x_3 = 5H/8$ between the 90-deg lamina and a neighboring 0-deg lamina. This behavior is unlike that of $\bar{\sigma}_{13}$, which attains its maximum value at the bottom surface of the PZT actuator. Numerical results for the mechanical displacement, components of the stress tensor, electric potential, and electric displacement at specific points in the laminate are given in Table 4 for $L/H = 5$. These can be used to compare predictions from various plate theories and finite element solutions.

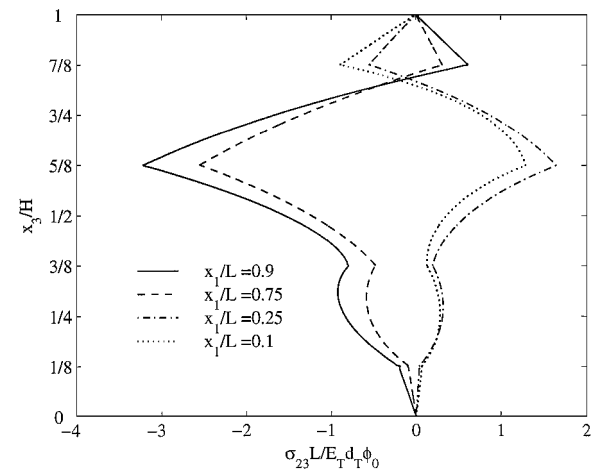
Figure 4 exhibits the variation of the electric potential on the surface $x_3 = 0$ of the PZT sensor when the mechanical load is applied on the upper surface of the laminate. When the edges are simply supported, a sinusoidal mechanical load on the top surface results in a sinusoidal electric potential at the bottom surface. However, such is not the case for a cantilever laminate. The electric potential exhibits boundary layers near the clamped edges, akin to those in a purely mechanical problem.²⁴

B. Piezoelectric Bimorph

Consider a cantilever piezoelectric bimorph^{33,34} structure consisting of two piezoelectric layers made of the same material bonded together as shown in Fig. 5. The two layers are mechanically bonded with an intervening electrode, as well as electrodes on the top and bottom surfaces. Application of a voltage to the outer surfaces induces an electric field of opposite sign in the neighboring layers. This causes one layer to expand and the other to contract, thus forcing the piezoelectric bimorph to bend. Tzou³⁴ has studied the use of a piezoelectric bimorph as fingers of a robot gripper. The gripper consists of two bimorphs placed slightly apart. The application of voltages of opposite sign to the bimorph fingers causes it to grip an object that is released when the applied voltage is switched off. Such robot grippers are ideally suited for gripping delicate objects, such as electronic chips, in high-precision operations. Piezoelectric bimorphs can also be used for microactuation. Tzou³⁴ used the



a) Mechanical load



b) Electrical load

Fig. 3 Transverse shear-stress distribution on four sections for a cantilever angle-ply hybrid laminate ($L/H = 5$).

finite element method to study the problem but did not report the interlaminar stresses.

The mechanics of deformation of a piezoelectric bimorph is similar to that of a bimetallic strip subjected to uniform heating. In the beam theory analysis of Timoshenko,³⁵ and later Boley and Weiner,³⁶ only the longitudinal stress is taken as nonzero and constant along the length of the strip. Timoshenko³⁵ noted that the interfacial shear and normal stresses are negligible in the interior of the strip but significant near the ends. Later investigators have

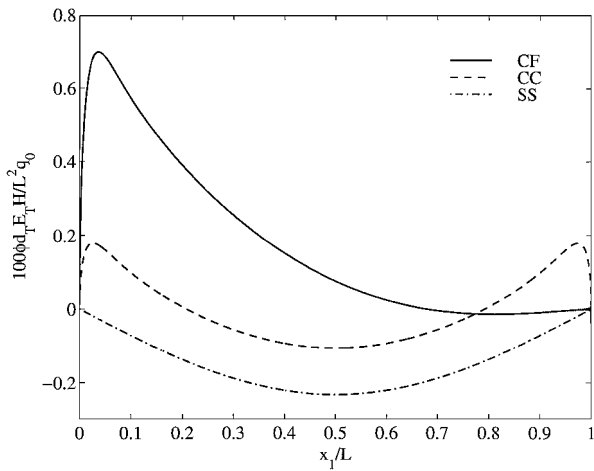


Fig. 4 Potential induced in the sensor at $x_3 = 0$ for a cross-ply hybrid laminate under mechanical load and corresponding to three boundary conditions ($L/H = 5$).

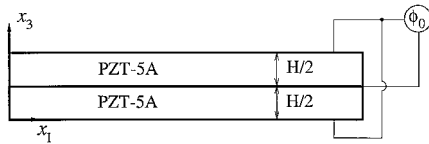


Fig. 5 Cantilever piezoelectric bimorph in parallel connection.

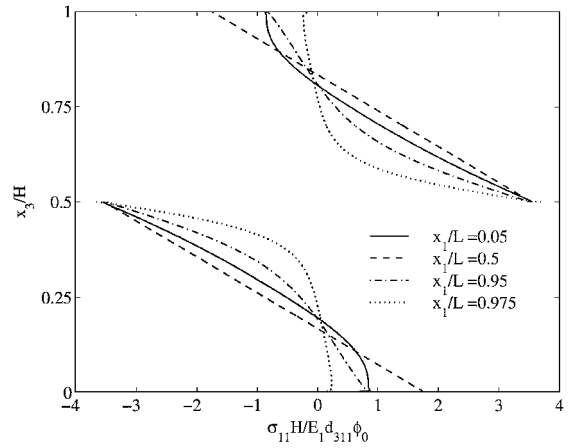
attempted to predict the interfacial stresses by employing improved analytical approximations and finite element analysis.^{37,38} Here we study the edge effects in piezoelectric bimorphs. Specifically, we are interested in the interfacial stresses because they are usually responsible for the failure of the bimorph.

The top and bottom surfaces are free of traction and subjected to an electric potential ϕ_0 . The interface $x_3 = H/2$ is electroded and maintained at zero electric potential, i.e., interface conditions (6) are enforced with $f(x_1) = 0$. The assumption is made that the normal component of the electric displacement D_1 vanishes at the edges $x_1 = 0, L$. Recalling that $K = 500$ provided convergent results for the problem studied in Sec. V.A, here we have chosen $K = 600$ to ensure sufficient accuracy of the results.

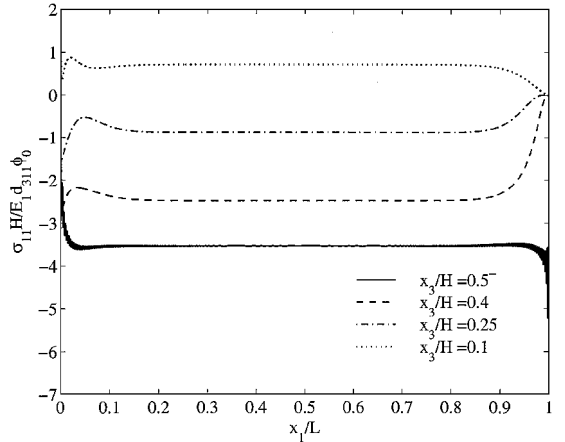
The beam theory approach of Boley and Weiner³⁶ or the Kirchhoff plate theory analysis outlined by Pionke and Wempner³⁸ can be easily modified for piezoelectric bimorphs by identifying the thermal strains with the piezoelectric strains. The transverse deflection \bar{u}_3 thus obtained for a piezoelectric bimorph is

$$\bar{u}_3(x_1) = 3d_{311}\phi_0(x_1/H)^2 \quad (30)$$

The normalized transverse tip deflection given by the beam theory for $L = 5H$ is $\bar{u}_3(L)/d_{311}\phi_0 = 75$ and that for $L/H = 10$ equals 300. Our three-dimensional analysis for the same configuration gives $u_3(L, H/2)/d_{311}\phi_0 = 93.9$ and 380.3 for the two values of L/H . The discrepancy in the transverse deflections between the two theories may be attributed to neglecting, in the beam theory, edge effects, transverse shear deformations, and the influence of d_{333} and d_{113} . The beam theory is not expected to give good result for a span-to-thickness ratio of 5. It also predicts that the longitudinal stress varies in a piecewise affine manner through the thickness of the bimorph. Figure 6a depicts the through-thickness variation of the longitudinal stress at four locations along the span; $E_1 = 61$ GPa and $d_{311} = -171 \times 10^{-12}$ m/V are the Young's moduli and the piezoelectric coefficient of PZT-5A.³² Whereas it is indeed piecewise affine at the midspan $x_1 = L/2$, there is considerable deviation in the profile at sections close to the clamped and free edges. In the beam theory the traction-free boundary condition at the edge $x_1 = L$ is satisfied in the sense that the resultant force vanishes. Here, the longitudinal stress vanishes at all points on the surface $x_1 = L$. The distribution of the longitudinal stress on four horizontal planes is shown in Fig. 6b. It remains constant along the length of the strip except at points close to the clamped and free edges. As we approach



a) Through-thickness variation

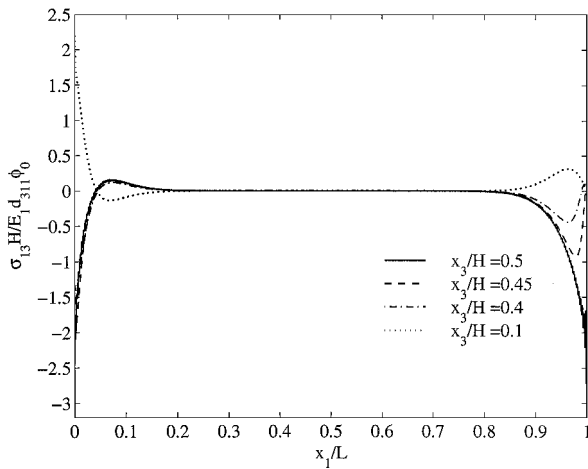


b) Axial variation

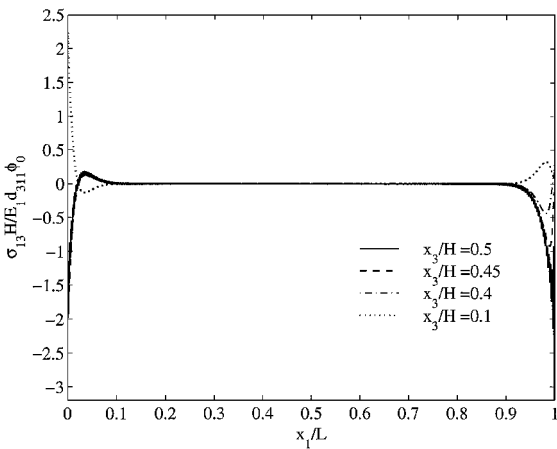
Fig. 6 Longitudinal stress in a cantilever piezoelectric bimorph ($L/H = 5$).

the free edge along the lines $x_3 = \text{constant}$, the longitudinal stress drops to zero, except on the interface. At the interface we see severe oscillations in the longitudinal stress near the edges. The distribution of the transverse shear stress on four horizontal surfaces of a bimorph is shown in Fig. 7 for span-to-thickness ratios $L/H = 5$ and 10. The results are plotted only for the bottom lamina because the through-thickness variation of σ_{13} is symmetric about the interface. As predicted by Timoshenko³⁵ for a bimetallic thermostatic strip, the transverse shear stress is negligible in the interior of the piezoelectric bimorph but significant near the ends. Most of the transverse shear stress is transferred in a region of one laminate thickness from the edges. The through-thickness distribution of the transverse normal stress is antisymmetric with respect to the interface. Thus, the transverse normal stress σ_{33} on the interface is identically zero. The axial distribution of the transverse normal stress on four planes is shown in Fig. 8. Like the transverse shear stress, it is also nonzero at points near the free edge. The magnitude of the transverse normal and shear stresses at points close to the edges is significantly more than that of the longitudinal stress there.

Figures 6b and 7 also show that the longitudinal stress and the transverse shear stress do not vanish at the point where the interface meets the free edge. This may be because of the presence of a singularity in the stress field at that point, which can be confirmed only by performing an asymptotic analysis. However, our truncated series solution seems to indicate the existence of a singularity and qualitatively captures the large stresses at that point. The stress singularity in a cantilever piezoelectric bimorph is similar to the free-edge singularity observed in laminated plates.³⁹ Here we have not performed a singularity analysis. Usually stress singularities occur at the point where two different materials meet a free edge. An edge singularity also exists in a bimorph even though both layers are made of the same material (PZT-5A).



a) $L/H = 5$



b) $L/H = 10$

Fig. 7 Transverse shear-stress distribution on four planes of a cantilever piezoelectric bimorph.

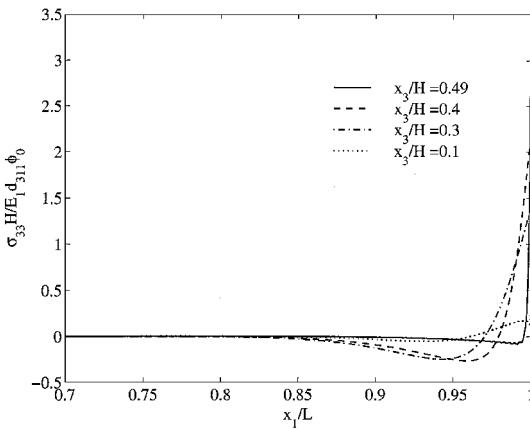


Fig. 8 Transverse normal stress on four planes of a cantilever piezoelectric bimorph.

C. Cantilever Plate with Surface-Bonded PZT Actuator Patches

The final example concerns a homogeneous 0-deg graphite-epoxy cantilever substrate with segmented PZT-5A actuators bonded to its upper and lower surfaces as shown in Fig. 9. This particular example has been considered by Crawley and de Luis³ and Crawley and Anderson⁴ who proposed two analytical models. The first model assumes a uniform extensional strain in the actuators and is called the uniform strain model. The second model includes extensional strain and bending in the actuators and is called the Euler-Bernoulli model.

The faces of the PZT actuators are electroded, and the interfaces at $x_3 = 0.1H, 0.9H$ are electrically grounded. If the surfaces $x_3 = 0, H$

are subjected to an identical electric potential ϕ_0 , the substrate will deform in bending. If electric potentials ϕ_0 and $-\phi_0$ are applied to the surfaces $x_3 = H$ and $x_3 = 0$, respectively, the substrate will deform in extension.

The surfaces $x_3 = 0.1H, 0.9H$ are subjected to two different kinds of boundary conditions along the span. The tractions are prescribed to be zero in the intervals $0 \leq x_1 \leq L/4$ and $3L/4 \leq x_1 \leq L$, whereas interface continuity conditions (6) are enforced in the interval $L/4 \leq x_1 \leq 3L/4$. To accommodate this change in the boundary conditions, we divide the substrate into three regions by introducing virtual vertical interfaces at $x_1 = L/4$ and $3L/4$. The continuity of mechanical displacements, tractions, electric potential, and normal component of electric displacement are enforced along these vertical interfaces. Because of the introduction of the vertical interfaces, there are five laminae with the same type of boundary condition on the entire length of each of its bounding surfaces. The vertical edges of the PZT are traction free and in contact with air, allowing us to prescribe $\sigma_1 = 0$ and $D_1 = 0$ on these surfaces. Recalling that $K = 500$ provided converged results for the first problem studied here, we take $K = 800$ terms for this example.

The distributions of the transverse displacements on three horizontal planes of the substrate are shown in Fig. 10a. The curves

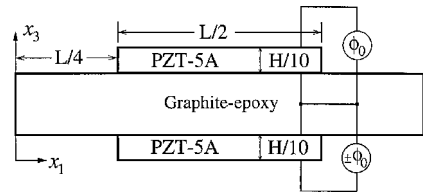
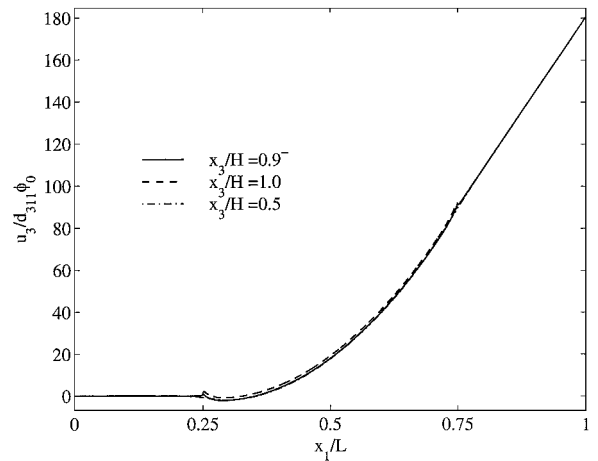
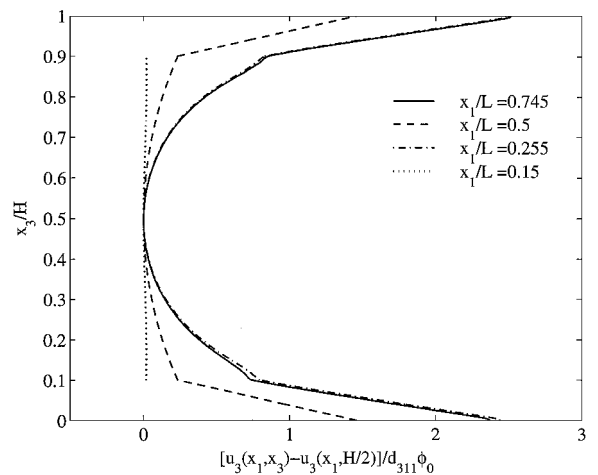


Fig. 9 Cantilever elastic substrate with segmented PZT actuators.



a) Axial variation



b) Through-thickness variation

Fig. 10 Transverse displacement in induced bending ($L/H = 10$).

corresponding to the midplane and the interface $x_3 = 0.9H$ overlap except at points close to the edges of the PZT actuator. The deviation of the transverse deflection of a point from that at the corresponding point on the midplane is shown in Fig. 10b. The transverse normal strain equals the derivative of these curves with respect to x_3 . In the Euler–Bernoulli theory the transverse normal strain is zero. Our results indicate that the transverse strains are significant at points close to the interfaces. The average elongation e of the normals to the midplane is defined as

$$e = \begin{cases} [u_3(x_1, 0.9H) - u_3(x_1, 0.1H)]/0.8H & \text{if } |x_1 - L/2| \geq L/4 \\ [u_3(x_1, H) - u_3(x_1, 0)]/H & \text{if } |x_1 - L/2| \leq L/4 \end{cases}$$

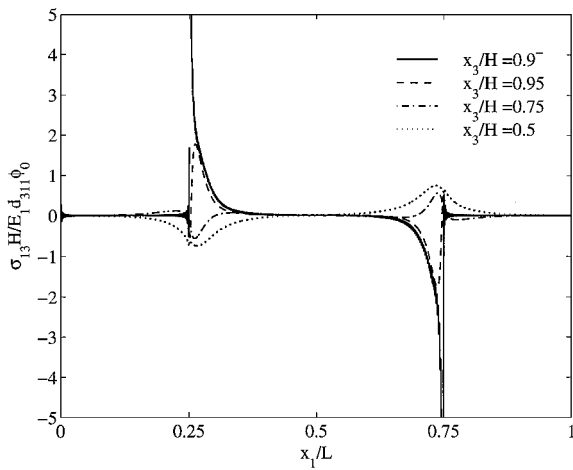
The average elongation is negligible at all locations along the span although the transverse normal strain is significant at points in the interval $|x_1 - L/2| \leq L/4$ because the transverse normal strain at a point in the upper half of the structure is negative of that at the corresponding point in the lower half, thus cancelling each other.

Transverse shear-stress distribution along the span on four planes is shown in Fig. 11a. The shear stress on the midplane of the substrate satisfies the continuity conditions across the artificial vertical interfaces that we introduced. The shear stress on the midsurface of the PZT drops to zero at the free edge as expected. The shear stress is very large at the corner points of the interface between the PZT and the substrate. The transverse normal stress plotted in Fig. 11b also exhibits large values at these points. These corners, when viewed asymptotically, are special points where a PZT wedge comes in contact with a graphite-epoxy surface. Because of the mismatch

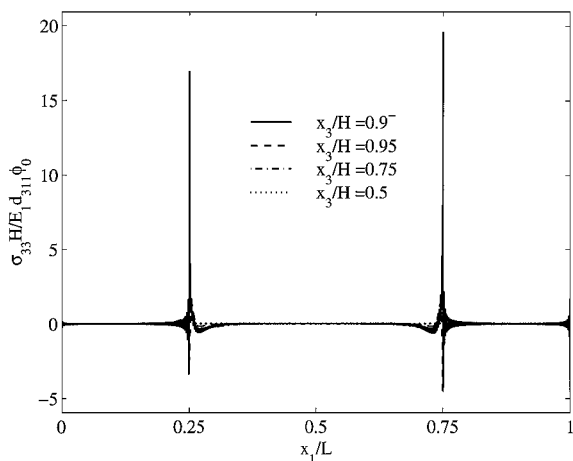
in the material properties, a stress singularity may exist at these corners.²⁸ The high shearing and transverse normal stresses can lead to debonding of the actuator from the substrate. Such large stresses were also observed at the edges of the PZT by Zhou and Tiersten²¹ and Batra et al.²³ Robbins and Reddy¹¹ analyzed a rectangular aluminium plate with a surface bonded actuator patch using a variable kinematic finite element model and obtained very large shearing and transverse normal stresses at the edges of the actuator. Xu and Noor³² also studied a rectangular laminated plate with an actuator

patch by employing a predictor-corrector finite element method but did not report the nature of the stresses at the edges of the patch.

The through-thickness variation of the transverse shear and longitudinal stresses for induced bending are shown in Figs. 12a and 12b, respectively, at four locations along the span of the laminate. The transverse shear stress attains large values near the interfaces and at the midplane in the interval $L/4 \leq x_1 \leq 3L/4$. It is negligible near the clamped and free edges. The longitudinal stress is also negligible at points close to the edges. As predicted by the Euler–Bernoulli model,⁴ at the midspan it exhibits a piecewise affine variation through the thickness. There is considerable deviation from this profile at points close to the edges of the PZT actuators. The normal stress curves at locations $x_1 = 0.3L$ and $0.7L$ overlap although the boundary conditions on the edges at $x_1 = 0$ and L are different.

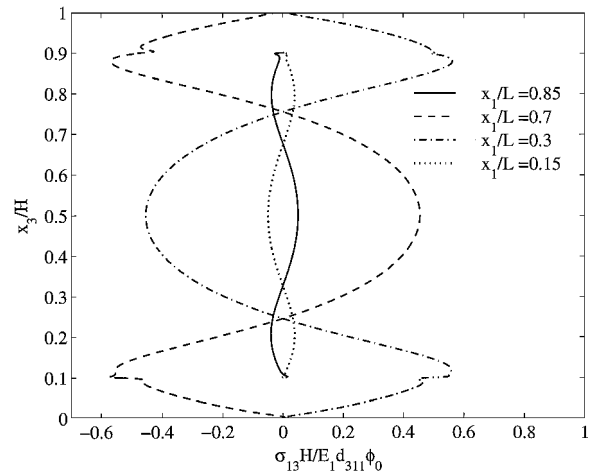


a) Transverse shear stress

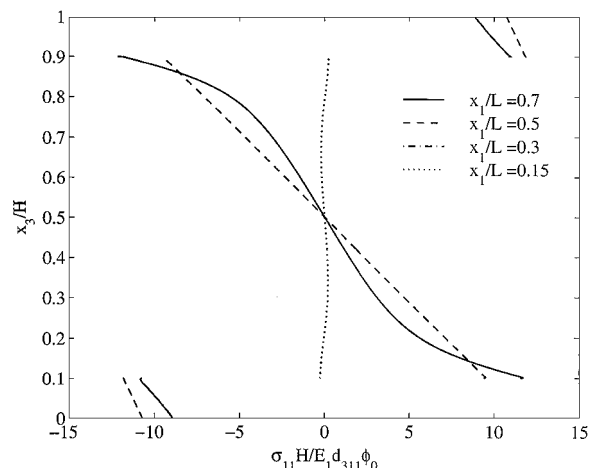


b) Transverse normal stress

Fig. 11 Axial variation of stresses on four planes in induced bending ($L/H = 10$).

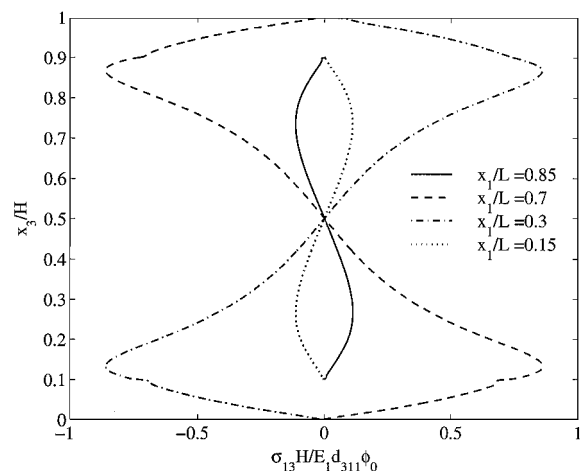


a) Transverse shear stress

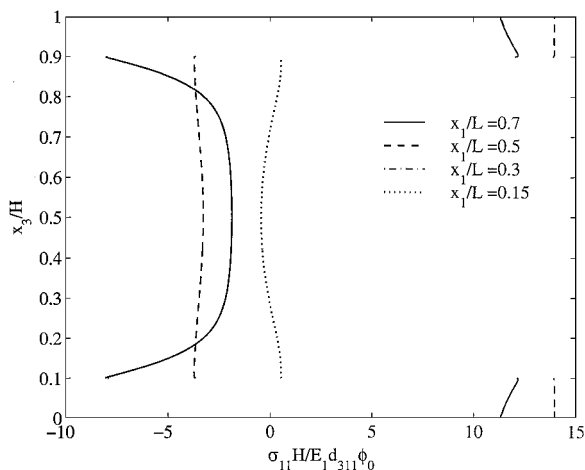


b) Longitudinal stress

Fig. 12 Distribution of stress on four sections in induced bending ($L/H = 10$).



a) Transverse shear stress



b) Longitudinal stress

Fig. 13 Distribution of stress on four sections in induced extension ($L/H = 10$).

We note that the uniform strain model and the Euler–Bernoulli model predict $u_{1,1}(L/2, 0.9H)H/d_{311}\phi_0 = -2.02$ and -2.15 , respectively, and the present three-dimensional solution gives -3.22 . Thus the axial strains given by the beam theory and the three-dimensional theory are quite different.

The through-thickness variation of the transverse shear and longitudinal stresses are shown in Figs. 13a and 13b for induced extension. The transverse shear stress attains a maximum value at points close to the interfaces and is negligible at points near the midplane. At the midspan $x_1 = L/2$ the longitudinal stress varies in a piecewise constant manner through the thickness. As observed in induced bending, the longitudinal stress curves corresponding to $x_1/L = 0.3$ and 0.7 overlap for induced extension. There is considerable deviation from the piecewise constant through-thickness variation predicted by the Euler–Bernoulli model⁴ near the edges of the PZT (cf. Fig. 13b).

We also studied a configuration with embedded PZT patches. For brevity these results are not shown here. For this case too, the transverse shear stresses are very large at points near the edges of the PZT. The distributions of the longitudinal stresses were qualitatively similar to that of surface-mounted PZT actuator patches.

We note that the results presented here will be quite good for a plate with the x_2 dimension much larger than the span of the plate. For rectangular plates the technique needs to be modified, e.g., see Vel and Batra.^{40,41}

VI. Conclusions

We have used the Eshelby–Stroh formalism to study the generalized plane deformations of a linear piezoelectric laminated plate. The three-dimensional equilibrium equations are exactly satisfied

at every point of the body. However, the boundary and interface continuity conditions are satisfied in the sense of Fourier series. By keeping a large number of terms in the series solution, displacements and stresses can be computed to any desired degree of accuracy. We have studied the deformations of cross-ply and angle-ply graphite-epoxy laminated plates with distributed PZT-5A layers bonded to its upper and lower surfaces and the composite laminate loaded either by an electric potential or by surface traction applied to the top-most surface with the bottom-most surface traction free. The effect of either clamping the edges, simply supporting them, or having them traction free has also been delineated. For a sinusoidal mechanical load applied to the top surface of the laminate, the variation of the electric potential in the PZT bonded to the bottom surface is sinusoidal only when the edges of the laminate are simply supported. The electric potential exhibits a boundary-layer effect near the clamped edges. In the case of a piezoelectric bimorph, the transverse stresses are transferred from one lamina to the other in a region of one laminate thickness from the edges. The stresses appear to be singular at the point where the interface meets the free edge. We also analyzed deformations and stresses in a graphite-epoxy cantilever beam with thin PZT patches bonded to its upper and lower surfaces at the center of the beam. The transverse shear and normal stresses are very large at the edges of the PZT-substrate interfaces. The transverse normal strains are also substantial in the PZT and the substrate. As illustrated by the results, the method is versatile and capable of analyzing piezoelectric plates subjected to arbitrary boundary conditions on the edges.

Acknowledgments

This work was partially supported by NSF Grant CMS9713453 and ARO Grant DAAG55-98-1-0030 to Virginia Polytechnic Institute and State University. R. C. Batra was also supported by an Alexander von Humboldt Award.

References

- Bailey, T., and Hubbard, J. E., "Distributed Piezoelectric-Polymer Active Vibration Control of a Cantilever Beam," *Journal of Guidance, Control, and Dynamics*, Vol. 8, No. 5, 1985, pp. 605–611.
- Im, S., and Atluri, S. N., "Effects of a Piezo-Actuator on a Finitely Deformed Beam Subjected to General Loading," *AIAA Journal*, Vol. 27, No. 12, 1989, pp. 1801–1807.
- Crawley, E. F., and de Luis, J., "Use of Piezoelectric Actuators as Elements of Intelligent Structures," *AIAA Journal*, Vol. 25, No. 10, 1987, pp. 1373–1385.
- Crawley, E. F., and Anderson, E. H., "Detailed Models of Piezoceramic Actuation of Beams," *Journal of Intelligent Material Systems and Structures*, Vol. 1, No. 1, 1990, pp. 4–25.
- Lee, C. K., "Theory of Laminated Piezoelectric Plates for the Design of Distributed Sensors/Actuators. Part 1: Governing Equations and Reciprocal Relationships," *Journal of the Acoustical Society of America*, Vol. 87, No. 3, 1990, pp. 1144–1158.
- Wang, B. T., and Rogers, C. A., "Laminate Plate Theory for Spatially Distributed Induced Strain Actuators," *Journal of Composite Materials*, Vol. 25, No. 4, 1991, pp. 433–452.
- Mitchell, J. A., and Reddy, J. N., "A Refined Hybrid Plate Theory for Composite Laminates with Piezoelectric Laminae," *International Journal of Solids and Structures*, Vol. 32, No. 16, 1995, pp. 2345–2367.
- Tzou, H. S., and Zhong, J. P., "Electroceramics and Vibrations of Piezoelectric Shell Distributed Systems," *Journal of Dynamic Systems, Measurement and Control*, Vol. 115, No. 3, 1993, pp. 506–517.
- Allik, H., and Hughes, T. J. R., "Finite Element Method for Piezoelectric Vibration," *International Journal for Numerical Methods in Engineering*, Vol. 2, No. 2, 1970, pp. 151–157.
- Robbins, D. H., and Reddy, J. N., "Analysis of Piezoelectrically Actuated Beams Using a Layer-Wise Displacement Theory," *Computers and Structures*, Vol. 41, No. 2, 1991, pp. 265–279.
- Robbins, D. H., and Reddy, J. N., "An Efficient Computational Model for the Stress Analysis of Smart Plate Structures," *Smart Materials and Structures*, Vol. 5, No. 3, 1996, pp. 353–360.
- Ha, S. K., Keilers C., and Chang, F. K., "Finite Element Analysis of Composite Structures Containing Piezoceramic Sensors and Actuators," *AIAA Journal*, Vol. 30, No. 3, 1992, pp. 772–780.
- Batra, R. C., and Liang, X. Q., "Finite Dynamic Deformations of Smart Structures," *Computational Mechanics*, Vol. 20, No. 5, 1997, pp. 427–438.
- Pagano, N. J., "Exact Solutions for Composite Laminates in Cylindrical Bending," *Journal of Composite Materials*, Vol. 3, No. 3, 1969, pp. 398–411.

- ¹⁵Pagano, N. J., "Influence of Shear Coupling in Cylindrical Bending of Anisotropic Laminates," *Journal of Composite Materials*, Vol. 4, No. 3, 1970, pp. 330–343.
- ¹⁶Ray, M. C., Rao, K. M., and Samanta, B., "Exact Analysis of Coupled Electroelastic Behavior of Piezoelectric Plate Under Cylindrical Bending," *Computers and Structures*, Vol. 45, No. 4, 1992, pp. 667–677.
- ¹⁷Ray, M. C., Bhattacharya R., and Samanta, B., "Exact Solutions for Static Analysis of Intelligent Structures," *AIAA Journal*, Vol. 31, No. 9, 1993, pp. 1684–1691.
- ¹⁸Ray, M. C., Rao, K. M., and Samanta B., "Exact Solution for Static Analysis of Intelligent Structures Under Cylindrical Bending," *Computers and Structures*, Vol. 47, No. 6, 1993, pp. 1031–1042.
- ¹⁹Heyliger, P., and Brooks, S., "Exact Solutions for Laminated Piezoelectric Plates in Cylindrical Bending," *Journal of Applied Mechanics*, Vol. 63, No. 4, 1996, pp. 903–910.
- ²⁰Brooks, S., and Heyliger, P., "Static Behavior of Piezoelectric Laminates with Distributed and Patched Actuators," *Journal of Intelligent Material Systems and Structures*, Vol. 5, No. 5, 1994, pp. 635–646.
- ²¹Zhou, Y. S., and Tiersten, H. F., "An Elastic Analysis of Laminated Plates in Cylindrical Bending due to Piezoelectric Actuators," *Smart Materials and Structures*, Vol. 3, No. 3, 1994, pp. 255–265.
- ²²Yang, J. S., Batra, R. C., and Liang, X. Q., "The Cylindrical Bending Vibration of a Laminated Elastic Plate due to Piezoelectric Actuators," *Smart Materials and Structures*, Vol. 3, No. 4, 1994, pp. 485–493.
- ²³Batra, R. C., Liang, X. Q., and Yang, J. S., "Shape Control of Vibrating Simply Supported Rectangular Plates," *AIAA Journal*, Vol. 34, No. 1, 1996, pp. 116–122.
- ²⁴Vel, S. S., and Batra, R. C., "The Generalized Plane Strain Deformations of Anisotropic Composite Laminated Plates," *International Journal of Solids and Structures*, Vol. 37, No. 5, 2000, pp. 715–733.
- ²⁵Tiersten, H. F., *Linear Piezoelectric Plate Vibrations*, Plenum, New York, 1969.
- ²⁶Eshelby, J. D., Read, W. T., and Shockley, W., "Anisotropic Elasticity with Applications to Dislocation Theory," *Acta Metallurgica*, Vol. 1, No. 2, 1953, pp. 251–259.
- ²⁷Stroh, A. N., "Dislocations and Cracks in Anisotropic Elasticity," *Philosophical Magazine*, Vol. 3, No. 4, 1958, pp. 625–646.
- ²⁸Ting, T. C. T., *Anisotropic Elasticity. Theory and Applications*, No. 45, Oxford Engineering Science Series, Oxford Univ. Press, New York, 1996.
- ²⁹Yang, X. X., Shen, S., and Kuang, Z. B., "The Degenerate Solution for Piezothermoelastic Materials," *European Journal of Mechanics. A, Solids*, Vol. 16, No. 5, 1997, pp. 779–793.
- ³⁰Dempsey, J. P., and Sinclair, G. B., "On the Stress Singularities in the Plane Elasticity of the Composite Wedge," *Journal of Elasticity*, Vol. 9, No. 4, 1979, pp. 373–391.
- ³¹Dube, G. P., Kapuria, S., and Dumir, P. C., "Exact Piezothermoelastic Solution of Simply-Supported Orthotropic Flat Panel in Cylindrical Bending," *International Journal of Mechanical Sciences*, Vol. 38, No. 11, 1996, pp. 1161–1177.
- ³²Xu, K., and Noor, A. K., "Predictor-Corrector Finite Element Approach for Electroelastic Analysis of Hybrid Composite Plates," *Computer Methods in Applied Mechanics and Engineering*, Vol. 147, Nos. 1–2, 1997, pp. 139–145.
- ³³Moulson, A. J., and Herbert, J. M., *Electroceramics: Materials, Properties, Applications*, Chapman and Hall, London, 1990.
- ³⁴Tzou, H. S., "Development of a Light-Weight Robot End-Effector Using Polymeric Piezoelectric Bimorph," *Proceedings of the 1989 IEEE International Conference on Robotics and Automation*, IEEE Computer Society Press, Silver Spring, MD, 1989, pp. 1704–1709.
- ³⁵Timoshenko, S. P., "Analysis of Bi-Metal Thermostats," *Journal of the Optical Society of America*, Vol. 11, Sept. 1925, pp. 233–255.
- ³⁶Boley, B. A., and Weiner, J. H., *Theory of Thermal Stresses*, Wiley, New York, 1960.
- ³⁷Suhir, E., "Interfacial Stresses in Bimetal Thermostats," *Journal of Applied Mechanics*, Vol. 56, No. 3, 1989, pp. 595–600.
- ³⁸Pionke, C. D., and Wempner, G., "The Various Approximations of the Bimetallic Thermostatic Strip," *Journal of Applied Mechanics*, Vol. 58, No. 4, 1991, pp. 1015–1020.
- ³⁹Ting, T. C. T., and Chou, S. C., "Edge Singularities in Anisotropic Composites," *International Journal of Solids and Structures*, Vol. 17, No. 11, 1981, pp. 1057–1068.
- ⁴⁰Vel, S. S., and Batra, R. C., "Analytical Solution for Rectangular Laminated Thick Plates Subjected to Arbitrary Boundary Conditions," *AIAA Journal*, Vol. 37, No. 11, 1999, pp. 1464–1473.
- ⁴¹Vel, S. S., and Batra, R. C., "Three-Dimensional Analytical Solution for Hybrid Multilayered Piezoelectric Plates," *Journal of Applied Mechanics* (to be published).

A. Chattopadhyay
Associate Editor